Computational Materials Science 137 (2017) 282–288

Contents lists available at ScienceDirect

Computational Materials Science

journal homepage: www.elsevier.com/locate/commatsci

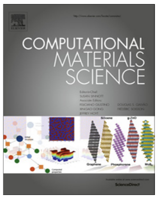

Revealing the deformation mechanisms of 6H-silicon carbide under nano-cutting

Zhonghuai Wu, Weidong Liu, Liangchi Zhang *

Laboratory for Precision and Nano Processing Technologies, School of Mechanical and Manufacturing Engineering, University of New South Wales, NSW 2052, Australia

ARTICLE INFO

Article history:
Received 27 April 2017
Received in revised form 31 May 2017
Accepted 31 May 2017
Available online xxxx

Keywords:
Silicon carbide
Nano-cutting
Molecular dynamics
Dislocation activation
Phase transformation
Ductile regime machining

ABSTRACT

6H silicon carbide (6H-SiC) is one of the most commonly used polytypes in commercial SiCs, such as its applications in high-temperature electronic devices, ultra-precision micro/nano dies and high-performance mirrors. However, the deformation mechanisms of 6H-SiC under nano-machining are unclear. This has significantly hindered the development of the material's ductile-regime and damage-free machining for micro/nano and miniaturized surfaces. This paper aims to explore such deformation mechanisms with the aid of large-scale molecular dynamics analysis. The results showed that with increasing the depth of cut 6H-SiC undergoes transition from elastic deformation to continuous plastic deformation and then to intermittent cleavage. A dislocation and structural analysis revealed that the plastic deformation of 6H-SiC can be realised *via* phase transformation from the Wurtzite structure to an amorphous structure, and/or through dislocations on the basal plane and/or pyramidal plane.

1. Introduction

Single crystal silicon carbide (SiC) is one of the most important ceramics and has been widely used in the applications that require high endurance [1]. Because of its excellent mechanical, thermal and chemical stabilities [2], for example, SiC is an ideal die material for precision micro/nano molding, is very suitable for fabricating semiconductor electronic devices that operate at high temperatures or high voltages [3], and has been used in high performance mirrors of infrared universe imaging systems [4]. However, the intrinsic brittleness and high hardness of SiC [5] have caused tremendous difficulties in the fabrication of ultra-precision micro/-nano components, such as in producing miniaturized functional surfaces.

The brittleness and ultra-hardness of SiC are associated with the strong covalent bonding, particularly the short sp3 bonding and closely packed diamond lattice structure [4]. At the nanoscale, however, it was reported that SiC could achieve uniform plastic deformation [6–9], which has led to further studies for achieving the ductile-regime machining of SiC [9–14]. For example, in the grinding of a single crystal 6H-SiC, Yin et al. [9] found a brittle-ductile transition with decreasing the diamond grit size. Patten et al. [14] also demonstrated a ductile material removal on single crystal 6H-SiC by single-point diamond turning.

Some studies have tried to clarify the underlying mechanisms of the nanoscale plasticity and brittle-ductile transition in SiC, both experimentally and numerically. Plasticity induced by amorphization was observed on 3C-SiC by using molecular dynamics (MD) simulations of nano-indentation and nano-scratching [15,16]. A phase transformation of sp3-to-sp2 order-disorder transition was also proposed based on some MD nano-cutting simulations on 3C-SiC [17–19]. With the aid of the MD nano-indentation simulations, Szlufarska et al. [20,21] found that the dislocations in 3C-SiC were first activated to initiate plastic deformation, and amorphization was due to the coalescence of the dislocation loops. Chen et al. [22] reported that dislocation activity should be the only plastic deformation mechanism of 3C-SiC. With increasing the depth of cut, Mishra and Szlufarska [23] found a transition of deformation regime of 3C-SiC from plowing to cutting with different categories of dislocations activated.

Compared with 3C-SiC, 6H-SiC has been more widely used in industry because it is easier to be produced [24]. However, there are only a few studies on 6H-SiC. Patten et al. [14,25] reported that they observed amorphous microstructure on a machined surface, and that the chips of 6H-SiC could be obtained under single-point diamond turning. They proposed a high-pressure phase transformation (HPPT) mechanism. Grim et al. [26] experimentally confirmed that basal dislocation could also be activated in the subsurface of 6H-SiC after mechanical polishing. It should be noted that 6H-SiC has a complicated Wurtzite structure, of which the dislocation/slip system is very different from that of 3C–SiC (a Zinc

---

* Corresponding author.
E-mail address: liangchi.zhang@unsw.edu.au (L. Zhang).

http://dx.doi.org/10.1016/j.commatsci.2017.05.048
0927-0256/

blende structure). Thus the deformation mechanisms and ductile-regime machining strategies developed for 3C-SiC cannot be simply applied to 6H-SiC.

To understand the possible mechanisms of plasticity of SiC, it is helpful to revisit the mechanics of plastic deformation. It is known [27] that to achieve a macroscopic homogeneous three-dimensional plastic deformation, five independent strain tensor components are required. This is because an arbitrary three-dimensional strain tensor has six independent components. However, when a material is incompressible during plastic deformation, one of the strain tensor components becomes redundant and only five of them are independent. Similarly, for a two-dimensional problem (plane-stress/strain), two independent strain tensor components are required. The minimum number of strain tensor components for the plastic deformation in ceramics and silicon can be through sufficient independent dislocation and twinning systems [28–31] or phase transformations [32–41]. In polycrystalline alumina, three independent slip systems (two basal and one prism) and two twin systems have been found to make the ductile regime machining possible. In single crystalline silicon, it has been clarified that the homogeneous plastic deformation in ductile-regime machining of the material is through structural transformations rather than dislocation glides [32–34,36–41]. Moreover, for materials of the Wurtzite structures such as BeO [42] and GaN [43], the plastic deformation mechanism is also via phase transformation. To date, however, it is still unclear whether sufficient slip systems or phase transformations can be initiated in 6H-SiC to produce at least five independent strain components, such that ductile-regime machining of the material is possible or not.

This paper aims to study the deformation mechanisms of 6H-SiC under noncutting. Particularly, the study tends to understand which deformation mechanism dominates the nanoscale ductility in the machining of 6H-SiC, and how possible mechanisms evolve with the depth of cut. A series of nano-cutting simulations with the aid of large-scale molecular dynamics (MD) technique will be carried out on the (0001) basal plane of 6H-SiC along the $\langle \bar{1}\bar{1}20 \rangle$ direction, with different depths of cut from 0.5 nm to 3 nm.

2. Methodology

All MD simulations of nano-cutting in this study were conducted by the large-scale atomic/molecular massively parallel simulator (LAMMPS) [44]. Fig. 1a shows the established model consisting of a workpiece of 6H-SiC and a diamond cutting tool. The workpiece was divided into three different parts: a Newtonian atoms zone, a thermostatic atomic layer and a boundary atomic layer. The motions of the Newtonian atoms were controlled by the second Newton's law (NVE ensemble). The thermostatic atoms (NVT ensemble) were applied to maintain the equilibrium temperature of the whole model. The boundary atoms were fixed during the simulation processes to eliminate the rigid body motion of the system [33,34,45]. Considering that the modulus and hardness of diamond are much higher than those of 6H-SiC, the diamond cutting tool was assumed to be rigid. The Tersoff potential was used for modelling the atomic interaction in the SiC workpiece [46,47]. The interaction between the silicon carbide atoms and the diamond indenter atoms are described by the Morse potential [33,34].

The cutting processes were conducted on the (0001) basal plane (vertical to z axis) along direction $\langle 11\bar{2}0 \rangle$ (the *x* axis) as shown in Fig. 1a. The *y* axis of the workpiece is in the $\langle \bar{1}100 \rangle$ crystallographic direction (see Fig. 1b). To reduce the computation time, periodic boundary condition was applied in the *y*-direction while fixed boundary conditions were used in *x*- and *z*-direction. The MD simulation model was first relaxed at 300 K. After relaxation, the cutting tool advanced with a speed of 100 m/s, which is in the range of a typical cutting speed in MD simulations [18,48,49]. The detailed simulation parameters and model dimensions are listed in Table 1. To study the changes of deformation mechanism of 6H-SiC, four different depths of cut were selected, i.e., 0.3 nm, 0.5 nm, 2 nm and 3 nm.

The MD results were visualized and analyzed by using OVITO [50]. The dislocations were analyzed by the dislocation extraction algorithm (DXA) [51]. Phase transformations were identified by the radial distribution function and bond angle distribution analysis.

3. Results and discussion

3.1. Deformation and chip formation

Fig. 2a to d shows the deformation and chip formation of 6H-SiC workpieces under nano-cutting at four different depths of cut. For the convenience of comparison, a uniform cutting length of 18 nm was used in all the cases. In the figures, red[1] and green atoms correspond to carbon and silicon atoms in the 6H-SiC workpiece, respectively. The carbon atoms of the diamond cutting tool, however, are indicated by yellow. The cyan atoms are those that have lost their positions in their initial diamond structure during nano-cutting, which have become 'non-diamond structural atoms'. Those colored in black represent the surface atoms of the SiC workpiece.

It is clear that the deformation and chip formation of 6H-SiC workpiece vary with the depth of cut, *d*. At $d = 0.3$ nm (Fig. 2a), no chip was formed. The subsurface was deformed by the cutting tool, but after the tool passed over, the workpiece material returned to their original diamond structure, except a small zone at the first tool-workpiece engagement. This indicates that the deformation of 6H-SiC was purely elastic when the nano-cutting entered its steady stage.

At $d = 0.5$ nm (Fig. 2b), ploughing (without material removal) occurred first, but it transferred to cutting with a chip formed. During the cutting, the atomic bonds of several layers of machined surface atoms had lost their originally diamond crystalline lattice structure. Moreover, a long and narrow deformation/structural transformation regime was formed in the subsurface.

Unlike the above cases at a small depth of cut, when *d* was increased to 2 nm and 3 nm (as shown in Fig. 2c and d), the cutting processes were with steady chipping and subsurface structural transformation. Moreover, crystalline clusters (highlighted by the arrows in Fig. 2c and d) and a small deformation/structural transformation zone ahead of the cutting tool (circled in Fig. 2c and d) emerged. It is also interesting to notice that at the cutting of $d = 3$ nm, a small atomic cluster within the chip could retain their original diamond crystalline lattice structure (see the enlarged part in Fig. 2d). The presence of such crystalline atoms within the chip could be due to the severe plastic deformation of surrounding material, which could be taken as a precursor of nano-cleavage [52].

As stated above, the cyan atoms in Fig. 2 are those that had lost their initial positions in the diamond structure. However, the new structures they formed are unclear. This will be elaborated in Sections 3.2 and 3.3 below.

3.2. Dislocation analysis

The resultant defect surfaces and dislocations are shown in Fig. 3a to d, corresponding to Fig. 2a to d, respectively. Fig. 3e is

---

[1] For interpretation of color in Fig. 2, the reader is referred to the web version of this article.